2023 IEEE/ASME International Conference on
Advanced Intelligent Mechatronics (AIM)

# AFM SMILER: A Scale Model Interactive Learning Extended Reality Toolkit for Atomic Force Microscopy Created with Digital Twin Technology

Fangzhou Xia[1,*], Shane Lovett[1], Eyan Forsythe[1], Malek Ibrahim[1], and Kamal Youcef-Toumi[1]

***Abstract*—Atomic force microscope (AFM) is a precision mechatronic system for nanoscale imaging of surfaces. Due to limited instrument access and lack of visualization techniques, understanding its principles can be challenging. Digital twin technology allows the creation of virtual representations of physical systems, which can be particularly useful to address challenges in AFM education. To realistically simulate nanoscale physics, we first developed new efficient algorithms for four virtual scale models, including cantilever mechanics, probe transducers, controller tuning, and contact mechanics. Second, three simulated experiment interactive learning modules are developed for instrument operation, including virtual imaging, system overview, and imaging modalities. In the end, three hardware systems are integrated for an extended reality experience, including a macroscopic AFM scale model, a haptic device for probe-sample interaction force feedback and an upgraded low-cost educational AFM for nanoscale imaging and instrumentation. This completes the eight total modules for the AFM SMILER: A Scale Model Interactive Learning Extended Reality toolkit. Preliminary studies shows the toolkit being helpful for AFM education. In addition to mechatronics and nanotechnology education, techniques developed in this work can be generally applied to computationally efficient realistic digital twin creation.**

***Index Terms*—Digital twin, scale model, actuators and sensors, nanotechnology, precision engineering, control, simulation, atomic force microscopy**

## I. INTRODUCTION

Atomic force microscope is a nanoscale surface characterization instrument widely used in a number of research fields. During imaging, a cantilever probe interacts with the sample in a controlled manner to extract the information. AFM is a versatile instrument that can operate in various environments and offers various modalities beyond topography imaging.

Digital twin is a powerful technology to create simulated objects in the metaverse. The combination of digital twin and internet-of-things sensors have found numerous applications in manufacturing plants, supply chain, healthcare, etc. A digital representation of physical systems allows rich user interaction in the virtual space, which is especially useful for training purposes. However, the level of details involved in creating digital twins can affect computational complexity significantly. For realistic simulation, researchers have tried to create digital twins for materials on the fundamental level [1].

[1] Massachusetts Institute of Technology Mechatronics Research Laboratory, 02139, Cambridge, MA, USA

[*] Corresponding author: Fangzhou Xia, email: xiafz@mit.edu



Training novice users to understand and operate an AFM can be challenging in several ways. First, a number of complex physical principles are involved during AFM imaging. Second, nanoscale AFM tip-sample interactions are hard to visualize. Third, the time each student can operate the instrument is limited due to resource constraints. Fourth, handling of the small cantilever probe and improper control parameter tuning may cause damage in the sample or probe.

To address these challenges, new educational tools are needed. Using digital twin technology in this work, we developed AFM SMILER: a Scale Model Interactive Learning Extended Reality toolkit. This toolkit focuses on interactive learning to allow guided exploration of various aspects of the AFM instrument both in principle and through practice. To empower digital twin technology, we integrated concept of scale models and extended reality with efficient algorithms for nanoscale process simulation.

Scale model is an important concept widely used for design visualization or engineering system studies to replace the real system. Scale models can be created both virtually or physically. For example, virtual scale models are widely used in the field of architecture for planning before construction. Physical scale models such as miniaturized wind tunnels are created to study aerodynamics of buildings or planes in an affordable manner [2]. To understand AFM principles, scale models can be very helpful for visualizing nanoscale processes.

Another critical feature to promote in-depth understanding is to use extended reality (ER). ER technologies have recently reached the level of maturity to become useful in fields such as robotic surgery [3], nanotechnology education [4] and experiential learning [5]. For example, VR models have been developed to evaluate pushing of cylindrical nanoparticles [6], predict nanolithography [7] results, and simulate nanomanipulation tasks [8] using nanoscale contact mechanics models. To get a realistic feeling of the tip-sample interaction force, researchers have mapped the measured cantilever deflection to haptic feedback devices and used the device for probe sample interaction control [9] and manipulation tasks [10]. This aspect is further explored in this work for extension to AFM dynamic mode operation and imaging, where the process is simultaneously visualized in a virtual simulator with force reproduced on a haptic hardware as a mixed reality experience.

Creation of the AFM SMILER builds upon our previous work on physical intelligence in the metaverse [11] and active probe educational AFM [12]. Several new capabilities and modules are developed to complete its functionality. An

overview of the AFM SMILER toolkit is shown in Fig. 1 to illustrates the main software modules and their interactions with hardware systems. The main contributions of this work can be summarized into three aspects.

1) Theoretical derivation of combined analytical and numerical methods for efficient simulation study of AFM contact mode and indentation force curve. Such methods are used to create four AFM SMILER virtual scale model modules: (a) cantilever mechanics, (b) probe transducer, (c) controller tuning, (d) contact mechanics.
2) Integration of hardware and software modules of the AFM SMILER software in Unity for interactive learning experiments including four instrument operation modules: (e) system overview, (f) virtual imaging, (g) imaging modalities, (h) hardware interaction.
3) Hardware development: (i) integration of a macroscopic AFM, (ii) interface with a haptic force feedback device, (iii) upgrade of a low-cost educational AFM for extended reality interaction.

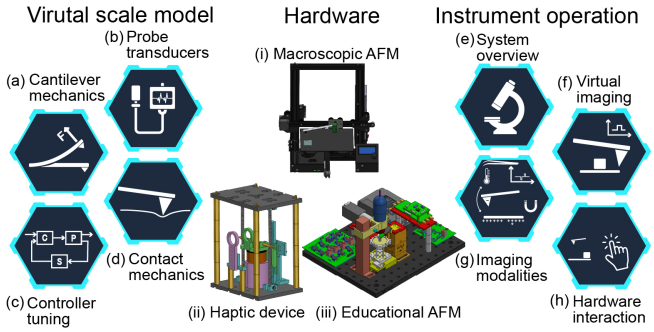


Fig. 1. AFM SMILER toolkit overview: integration of virtual scale models and instrument operation simulators to promote conceptual understanding and interactive learning using digital twin technology (cyan arrows indicating data exchange between hardware and simulator modules)

The paper is organized as follows. In section II, the virtual scale models for illustration of AFM cantilever mechanics and transducer principles are introduced briefly based on prior results in [11]. The focus of discussion is then placed on the simulation of more complex scale models on AFM imaging controller tuning and contact mechanics in section III. Section IV focuses on interactive learning modules, including system 3D models, virtual AFM imaging experiments, and various imaging modalities. Details of hardware systems designed for extended reality interaction are covered in section V including a macroscopic AFM, a haptic force feedback device and a low-cost educational AFM. For section VI, a preliminary educational study of AFM SMILER is presented with survey results from students. In the end, we conclude by illustrating broader applications of the AFM SMILER design strategy and future works to make the toolkit widely accessible.

## II. VIRTUAL SCALE MODEL ILLUSTRATION

Understanding nanoscale systems can be challenging due to the lack of proper visualization. As a result, nanoscale functional materials used in AFM probes as transducers are difficult to comprehend for novice users. Virtual scale models in the simulation environment allow direct visualization of the principles and an improved interactive learning experience.

### A. Cantilever Mechanics

At the core of the AFM is a microcantilever probe that interacts with the sample surface. Understanding its mechanics is important for the design of sensors for deflection measurement and actuators for cantilever resonance excitation.

For a cantilever with rectangular cross-sectional area, the deflection $z(x)$ and angle $\theta(x)$ in the vertical $z$ direction at each point along the axial direction $x$ with the fixed end at origin can be derived as in Eq.(1). The generic formula for the internal stress $\sigma_{xz_b}$ at location $x$ and height $z_b$ from the neutral axis of the cantilever is also provided in Eq.(1).

$$\begin{cases} z(x) = \frac{F\ell^3}{6EJ}\left[3\left(\frac{x}{\ell}\right)^2 - \left(\frac{x}{\ell}\right)^3\right] \\ \theta(x) = \frac{F\ell^2}{2EJ}\left[2\left(\frac{x}{\ell}\right) - \left(\frac{x}{\ell}\right)^2\right] \\ \sigma_{xz_b} = -Ez_b\frac{d^2z}{dx^2} \end{cases} \tag{1}$$

where the involved physical parameters: length $\ell$, width $w$, thickness $h$, uniform density $\rho$, and Young's modulus $E$.

Using these parametric relations, the 3D model of a microcantilever can be scaled up in the virtual simulator environment directly. For Unity implementation consideration, two modifications are made to ensure appropriate visualization: (1) the calculated cantilever deflection is scaled by 100 times in the vertical direction to make the deflection more significant; (2) the animated cantilever deflection is discretized into 100 steps in each direction for visualization since rigging of the 3D model with the exact deflection curve is challenging. As shown in Fig.2(a-b), with a force input acting on the probe tip, the deflection, internal stress and strain along the cross section area at various location are visualized in AFM SMILER.

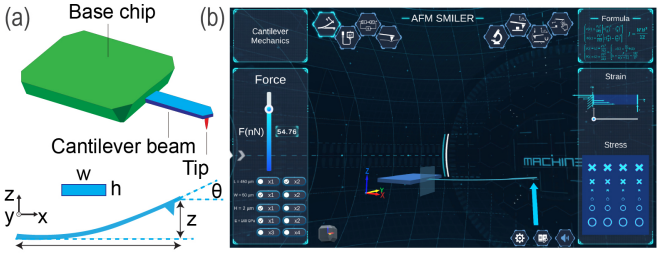


Fig. 2. AFM cantilever transducer principle virtual scale models: (a) cantilever mechanics, (b) cantilever mechanics in AFM SMILER

### B. Probe Transducer Principles

In conventional AFM, an optical beam deflection system is utilized to convert the cantilever free end angle into linear motion of the reflected laser spot on a quadrature photodiode. For small deflection, the angle is directly proportional to the vertical tip deflection and subnanometer resolution can be achieved. For actuation, a piezo actuator is placed in the cantilever holder to acoustically excite the cantilever resonance.

Going beyond conventional AFMs, the microcantilever deflection can be measured using six sensing principles. For dynamic mode operation where cantilever resonance excitation is needed, six actuation principles have also been utilized.

Cantilevers with nanofabricated sensors and actuators using functional materials embedded in the probe is considered as an active probe. A summary of all 12 transducer principles is provided in Table I. More details of the sensing principles can be found in our previous work at [11].

TABLE I
CANTILEVER TRANSDUSER PRINCIPLES

| Physical principle | Function | Signal | Size |
|---|---|---|---|
| Optical beam deflection | Sensing | DC&AC | Bulk |
| Astigmatic detection | Sensing | DC&AC | Bulk |
| Interferometry | Sensing | DC&AC | Bulk |
| Piezo-acoustic | Actuation | AC only | Bulk |
| Photothermal | Actuation | DC&AC | Bulk |
| Electromagnetic | Actuation | DC&AC | Bulk |
| Electrostatic | Actuation | DC&AC | Bulk |
| Optomechanical | Sensing | DC&AC | Embedded |
| Piezoresistive | Sensing | DC&AC | Embedded |
| Electrothermal | Actuation | DC&AC | Embedded |
| Piezoelectric | Both | AC mostly | Embedded |

With the micrometer scale cantilever probe and various physical principles involved, an interactive visualization tool is desirable to visualize the transducers. Virtual 3D scale models are created to better illustrate these principles using analytical formula derived in [11],

## III. EFFICIENT SCALE MODEL SIMULATION

Scale model creation with complex interactions is computationally more challenging. One important feature offered by a digital twin is its capability to simulate the behavior of the physical system and make decisions on how to adjust controller parameters. While realistic simulations of the AFM system on the nanoscale is possible with software packages like Virtual Environment for Dynamic AFM (VEDA) [13] or Matlab [14], it requires nanosecond time step during the numerical integration, which makes it computationally too expensive to be simulated especially in real time. For the AFM SMILER toolkit, we developed simplified models to capture the main physics using combined analytical and numerical techniques for simulation as described in this section.

### A. Imaging Controller Tuning

In most AFM imaging experiments, the PID feedback controller parameters need to be adjusted manually to ensure good tracking of the sample topography. Novice AFM users without sufficient background knowledge in control systems can incorrectly tune the parameters to make the system unstable that may damage the probe or the sample. With limited instrument accessibility and potential risk of probe/sample damage, exploring parameter tuning in simulation before using the actual instrument can be beneficial.

For illustration purposes, we modeled the constant force contact mode AFM imaging dynamics with the cantilever deflection regulated by a PID controller to a desired setpoint. For typical AFM imaging experiments with scan speed at several lines per second, the topography variation frequency is much lower than the scanner resonance and therefore the input force/voltage to displacement dynamics of the nano-positioner can be ignored. In the out-of-plane direction, the cantilever and the sample can each be modeled as a second-order mass-spring-damper system, as shown in Fig.3. This model assumes that the cantilever probe tip remains in contact with the sample to capture the main dynamics, and nanoscale non-linear effects are ignored to obtain analytical solutions.

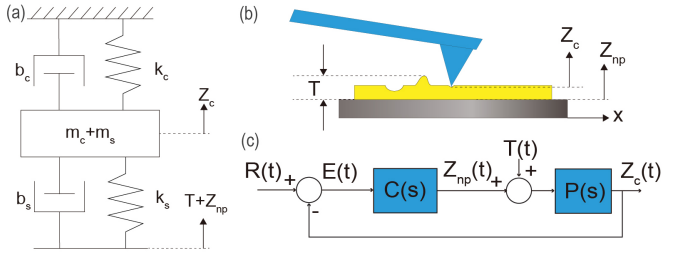


Fig. 3. An AFM constant force contact mode dynamics model: (a) a lumped parameter model of contact mode AFM out-of-plane dynamics, (b) a cantilever brought into contact with a sample with illustration key variables, (c) a block diagram of the AFM out-of-plane control system

During an imaging experiment, the cantilever deflection $Z_c$ is measured. The error signal with respect to a reference setpoint $R$ is used to adjust relative probe-sample distance through the nano-positioner height $Z_{np}$. The sample topography variation $T$ can be viewed as an external time-dependent disturbance signal related to the in-plane scan speed, which needs to be compensated by the PID controller. The transfer function of the plant $P(s)$ is given in Eq.(2). With a standard PID controller transfer function $C(s) = K_p + \frac{K_I}{s} + K_D s$, the transfer function $Z_c$ and $Z_{np}$ with respect to the topography disturbance input $T$ is shown in Eq.(3).

$$P(s) = \frac{b_s s + k_s}{(m_c + m_s)s^2 + (b_c + b_s)s + (k_c + k_s)} \tag{2}$$

$$\begin{cases} \frac{Z_c}{T} = \frac{b_s s^2 + k_s s}{As^3 + Bs^2 + Cs + D} \\ \frac{Z_{np}}{T} = -\frac{b_s K_D s^3 + (K_D K_S + b_s K_p)s^2 + (K_P k_s + K_I b_s)s + K_I k_s}{As^3 + Bs^2 + Cs + D} \end{cases} \tag{3}$$

$$A = m_c + m_s + b_s K_D, \quad B = b_c + b_s + K_D k_s + b_s K_p$$
$$C = k_c + k_s + K_p k_s + K_I b_s, \quad D = K_I k_s$$

where the system mass $m$, spring $k$ and damper $b$ parameters have subscripts $s$ for sample and $c$ for cantilever. The PID controller has proportional gain $K_P$, integral gain $K_I$ and derivative gain $K_D$. $A, B, C, D$ are dummy variables.

The transfer function of $Z_c$ and $Z_{np}$ with respect to the reference setpoint $R$ can also be derived. However, since $R$ is configured before probe-sample engagement and typically remains unchanged during imaging, the final value theorem can be applied to obtain the steady-state response as in Eq.(4).

$$\begin{cases} Z_c^{ss} = R \\ Z_{np}^{ss} = \frac{k_c + k_s}{k_s} R \end{cases} \tag{4}$$

The solution makes sense as the controller would allow the steady state cantilever deflection $Z_c^{ss}$ to track the reference setpoint $R$. The corresponding nano-positioner $Z_{np}^{ss}$ motion should be larger than the desired cantilever deflection $R$ since the sample can also deform during the interaction.

In principle, this linear transfer function can be solved with numerical integration by the sum of the responses to the time-dependent input $T(t)$ and the steady-state solutions to $R$. In practice, this would be very time-consuming with the small

time step (microseconds) needed, which can take millions of time steps for a single scan line.

As an alternative, we propose to approximate the input signal $T(t)$ with a series of polygon segments, which can be decomposed into sum of scaled and time-shifted step and ramp functions. Frequency domain analytical solutions for step and ramp inputs to the system can be calculated. Using inverse Laplace transform and superposition of these solutions in the time domain allows the recreation of AFM scan lines. Compared to numerical integration, the solution value at any target time can be obtained directly by superposition of analytical solutions without the need to go through all the history of the system from the beginning.

The main problem is now converted to obtaining the analytical solution through Laplace transform techniques. The simplest solution situation is for the system with $K_I = 0$ and unit step input. In this case, the overall transfer function is reduced to a second-order system. The solution assuming two distinct real roots $R_{1,2}$ (over-damped system) can be obtained analytically as shown in Eq.(5).

$$\begin{aligned} Z_c &= \frac{1}{s}\frac{b_s s + k_s}{As^2 + Bs + C} = \frac{1}{s}\frac{b_s s + k_s}{A(s-R_1)(s-R_2)} \\ &= \frac{1}{A}\left(\frac{X}{s} + \frac{Y}{s-R_1} + \frac{Z}{s-R_2}\right) \\ R_{1,2} &= \frac{-B \pm \sqrt{B^2 - 4AC}}{2A}, \quad X = k_s\frac{A}{C} = \frac{k_s}{R_1 R_2} \\ Y &= \frac{b_s R_1 + k_s}{R_1(R_1 - R_2)}, \quad Z = \frac{b_s R_2 + k_s}{R_2(R_2 - R_1)} \end{aligned} \tag{5}$$

Various other characteristic root situations exist for unit step and unit ramp inputs. For cases where $K_I \neq 0$, a third-order system needs to be factorized into components that match a form suitable for inverse Laplace transform. For the most complicated situation in this simulation, a ramp input to the third-order system yields a fifth order on the denominator. Fortunately, analytical solutions to cubic equations exist and an example solution with one real root and two complex conjugate roots is illustrated in Eq.(6).

$$\begin{aligned} Z_c &= \frac{1}{s^2}\frac{b_s s^2 + k_s s}{As^3 + Bs^2 + Cs + D} \\ &= \frac{1}{s^2}\frac{b_s s^2 + k_s s}{A(s-R_1)\left[(s+a)^2 + \omega_d^2\right]} \\ &= \frac{1}{A}\left[\frac{W}{s^2} + \frac{X}{s} + \frac{Y}{s-R_1} + \frac{Z\omega_d}{(s+a)^2+\omega_d^2} + \frac{\Gamma(s+a)}{(s+a)^2+\omega_d^2}\right] \end{aligned} \tag{6}$$

The coefficients $W, X, Y, Z, \Gamma$ in the partial fraction expansion can be obtained by matching the coefficients to form a system of five linear equations as shown in Eq.(7). Solution to such a linear system can be computed efficiently by the computer using algorithms such as Gauss-Jordan elimination. A total of 14 solution cases were derived for the second/third-order system dynamics with unit step or unit ramp inputs.

$$\begin{cases} X + Y + \Gamma = 0 \\ W + 2Xa - XR_1 + 2aY + Z\omega_d + \Gamma a - \Gamma R_1 = 0 \\ 2Wa - WR_1 + Xa^2 + X\omega_d^2 - 2XR_1 a + \ldots \\ \qquad \ldots + Ya^2 + Y\omega_d^2 - Z\omega_d R_1 - \Gamma a R_1 = b_s \\ Wa^2 + W\omega_d^2 - 2WR_1 a - XR_1 a^2 - XR_1\omega_d^2 = k_s \\ -WR_1 a^2 - WR_1\omega_d^2 = 0 \end{cases} \tag{7}$$

With frequency domain solution, the inverse Laplace transform is used to obtain the time domain analytical solution. The scaled and time-shifted summation of each individual inputs gives the time domain response of $Z_c$ and $Z_{np}$. The in-plane scan speed $V_i n$ determines the time domain shift of each input with the user-defined topography variation.

The AFM SMILER controller tuning simulation results of the algorithm are shown in Fig.4. The simulated cantilever deflection $Z_c$ and nano-positioner position commands $Z_{np}$ are visualized with both forward (trace) and backward (retrace) scan lines with good tracking performance. An example of good controller tracking is shown in Fig.4(a) with parameters shown in the column on the left. By adjusting the parameters, several realistic effects can be observed from the scan lines, including Fig.4(b): increased topography estimation error due to sample deformation when its stiffness is comparable to the cantilever ($k_c = k_s = 1$); Fig.4(c): trace and retrace topography tracking difference due to step-up/down change from opposite directions, which becomes more significant when line scan speed is increased from 10 $\mu m/s$ to 1000 $\mu m/s$; Fig.4(d): unstable oscillation due to large controller gain with $K_p = 100$ and $K_I = 100$. Note that the default unit of the simulation is set to $N = kg/(m/s^2) = ng/(m/\mu s^2)$ to match the typical AFM scales but can be adjusted generically for simulation.

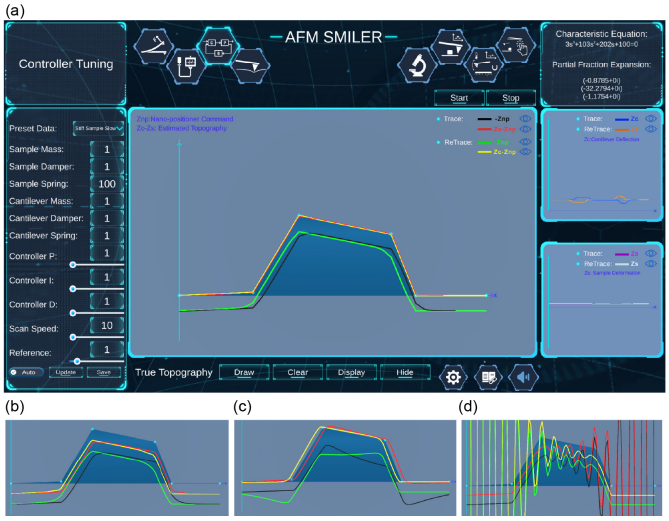


Fig. 4. Simulated scanning response in Unity for constant force contact mode AFM with inverted scanner command $-Z_{np}$ trace (black) and retrace (green) signals as well as estimated topography $Z_c - Z_{np}$ trace (red) and retrace (brown). Simulation results with different parameters: (a) main interface showing good tracking curves with high sample to cantilever stiffness ratio, stable controller and slow scanning speed as default parameter values, (b) low stiffness with large sample deformation ($k_s = 1$), (c) high scanning speed with poorer tracking ($V_i n = 1000$), (d) large controller gain with unstable oscillation ($K_P = K_I = 100,\ K_D = 0,\ b_s = b_c = 0.015$).

In AFM SMILER, users can explore the dynamic system models and optimize the controller. With millisecond level update rate, real-time parameter investigation can be conducted easily compared to VEDA [13] or Matlab [14] models, which can take several minutes to run. Without compromising the main dynamics, AFM SMILER solves tens system of linear equations with up to five unknowns from polygon point inputs, which is 4-5 orders of magnitude fewer steps compared to micro/nanosecond time steps in accurate numerical simulation.

### B. AFM Indentation Curve

In AFM operation, the force volume mode takes a force versus distance curve and fit a contact mechanics model to identify parameters. Finite element analysis models are typically used for detailed analysis of generic geometry but can again be computationally too expensive to implement.

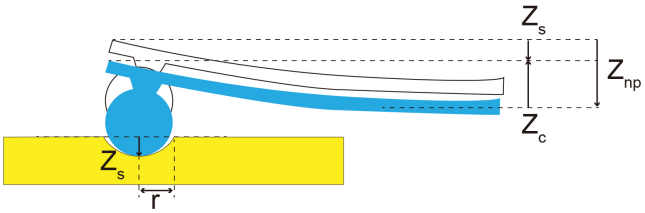


Fig. 5. Parameter definition of the Hertz model for an example spherical tip geometry used in the indentation curve analysis

To simulate this indentation process, we used Hertz and Sneddon model for four typical probe tip geometries. A set of four governing equations is used to describe the relations between four key variables, including the cantilever deflection $Z_c$, the sample deformation at the tip apex $Z_s$, the tip-sample interaction force $F_{ts}$, and the contact circle radius $r$, as defined in Fig.5. For a parabolic tip geometry with the radius of curvature $R_p$, the governing equation is given in Eq.(8).

$$\begin{cases} Z_{np} = Z_s + Z_c \\ F_{ts} = kZ_c \\ F_{ts} = \frac{4\sqrt{R_p}}{3}\frac{E}{1-\nu^2}Z_s^{3/2} \\ Z_s = \frac{r^2}{R_p} \end{cases} \tag{8}$$

$$\Rightarrow \qquad F_{ts} = k(Z_{np} - Z_s) = \frac{4\sqrt{R_p}}{3}\frac{E}{1-\nu^2}Z_s^{3/2} \tag{9}$$

where $E$ is the sample Young's modulus, $\nu$ is the sample Poisson's ratio, and $Z_{np}$ is the known sample nanopositioner $z$ axis displacement controlled during indentation. The system of equations is non-linear but fortunately it can be simplified to an expression about the sample deformation $Z_s$ as shown in Eq.(9). Since both sides of the expression have the physical meaning as tip-sample interaction force, they are both monotonic and the solution of $Z_s$ should be within the range of 0 to $Z_{np}$. As a result, a simple discretized binary search within the range would find the numerical solution quickly.

Similar results can be obtained for probe tip with spherical, conic and pyramid shapes as shown in Fig.6(a-d), where the last two formula in Eq.(8) are replaced. For spherical tip shape with radius $R$, the two equations are provided in Eq.(10)

$$\begin{cases} F_{ts} = \frac{E}{1-\nu^2}\left[\frac{a^2+R^2}{2}\ln\left(\frac{R+r}{R-r}\right) - rR\right] \\ Z_s = \frac{r}{2}\ln\left(\frac{R+r}{R-r}\right) \end{cases} \tag{10}$$

Similarly, for a cone with half opening angle of $\alpha$, the equations are shown in Eq.(11).

$$\begin{cases} F_{ts} = \frac{E}{1-\nu^2}\frac{2\tan\alpha}{\pi}Z_s^2 \\ Z_s = \frac{\pi}{2\tan\alpha}r \end{cases} \tag{11}$$

For the last common AFM tip geometry of a four-sided pyramid with face angle $\beta$, the relations are listed in Eq.(12).

$$\begin{cases} F_{ts} = \frac{E}{1-\nu^2}\frac{\tan\beta}{\sqrt{2}}Z_s^2 \\ Z_s = \frac{\sqrt{2}}{\tan\beta}r \end{cases} \tag{12}$$

An indentation curve simulation example is shown in Fig.6(e) with real-time animation by varying $Z_{np}$. Notice that the approach and retract section of the indentation curve would be the same for this simulation since only the elastic model is considered. In practice, the damping energy loss and adhesion would affect the results and curve-fitting techniques are used to identify the parameters. For numerical implementation, the default units used in the indentation curve contact mechanics module are scaled to nano-meter, nano-Newton and giga-Pascal to reduce the numerical error during computation.

To verify the accuracy of the simulator, the parameters for a sphere tip with parameters shown in Fig.6(e) are configured in the VEDA simulator [13] to check for the results. The VEDA simulator includes more parameters to include approaching speed cantilever dynamics and deformation at the tip. When approaching slowly and indenting on a sample much softer than the cantilever tip, the result obtained from our simulator and VEDA should be identical. With identical parameters, VEDA gives a result at around 0.70073 nm of observed deflection at the cantilever at 0.993 nm indentation and the AFM SMILER gives 0.7029 nm at 1 nm indentation. The two results are almost the same, indicating the correctness and accuracy of the AFM SMILER model implementation.

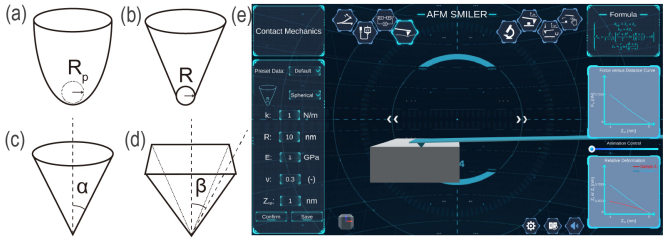


Fig. 6. AFM probe tip geometry illustration for (a) parabolic tip, (b) spherical tip, (c) conic tip, (d) pyramid tip and (e) simulated indentation curve for a parabolic tip geometry simulated in Unity without adhesion

## IV. INTERACTIVE LEARNING EXPERIMENTS

As scale model simulators provide a principle level understanding of the physics, virtual interaction with the instrument provides the practical user experience required to operate AFMs. Cost of commercial AFMs can easily go over tens of thousands of dollars, which means a limited number of instruments are available to the students for hands-on experiments. Moreover, novice users tend to make mistakes that may damage the sample or the probe, which leads to frustration in the learning process. To resolve these two problems, the interactive learning modules are designed to provide subsystem overview and simulate actual imaging experiments.

### A. AFM System Overview

The system overview module allows virtual disassembly of the AFM systems. This provides an under-the-hood view of the AFM typically impossible with real instruments. Two AFM systems are modeled in this module: (1) a conventional Bruker Multimode 8 AFM with optical beam deflection sensing and piezoacoustic actuation and (2) a low-cost educational AFM with piezoresistive sensing electrothermal actuation active probe developed previously in our group [12].

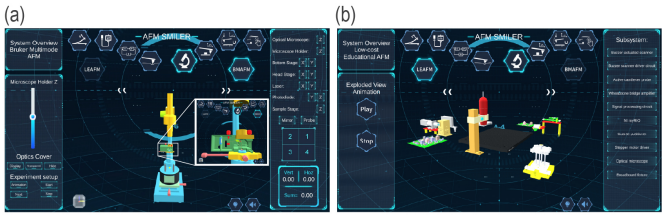


Fig. 7. System 3D model overview: (a) Bruker Multimode 8 overview and zoomed-in laser path alignment, and (b) educational AFM introduction

The Bruker AFM 3D model is created realistically with all laser alignment optics included, as shown in Fig.7 (a). Users can make the housing transparent and turn the nobs to get familiarized with the experiment setup process. A guided animation of the experiment setup process with audio description is also developed as a virtual lab manual that can be used before the actual experiment. The low-cost educational AFM module has similar functionalities with an exploded view animation screenshot shown in Fig.7 (b).

### *B. Virtual AFM Imaging Experiment*

After initial setup of the AFM, a scanning experiment can be conducted in the virtual AFM imaging module. First, previously scanned AFM images of real samples or artificially generated surface topography can be loaded into the system. After entering the imaging parameters, such as scan range, pixel resolutions, and scan speed. The virtual scanning process can be animated with constant height, constant force, or dynamic mode, as shown in Fig.8(a).

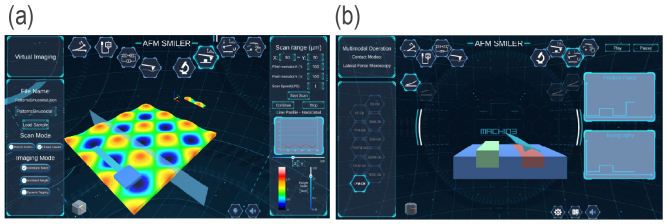


Fig. 8. AFM imaging simulator: (a) virtual imaging of a pre-loaded sample, (b) AFM imaging modality demonstration with lateral force microscopy.

### *C. Imaging Modalities*

One of the main strengths of AFM is its flexibility. A number of imaging modalities have been developed for the imaging of various surface properties. Based on the nature of the probe sample interaction dynamics, they can be categorized into contact modes, dynamic modes, jumping modes and hybrid modes. More details of the can be found in [15]. Animated illustrations of the imaging principles for these modes are implemented in the simulator. An example of the lateral force microscopy mode is shown in Fig.8(b). In this mode, the cantilever scans laterally over the sample with its deflection regulated and its twisting angle reflects the friction coefficient of the sample.

## V. EXTENDED REALITY HARDWARE DESIGN

Going beyond virtual simulation, merging extended reality hardware with AFM SMILER software would be helpful to promote a more memorable interactive learning experience. Three hardware systems have been developed including a Macroscopic AFM, a haptic force feedback device and a low-cost educational AFM. All three systems can interface with the local version of the AFM SMILER Unity simulator.

### *A. Macroscopic AFM*

A physical AFM scale model on the macroscopic scale can be helpful to illustrate the imaging process. Real AFM images of 3D nanoscale sample surfaces can be converted to STL files and 3D printed as mesoscale samples and re-imaged using the macroscopic AFM. Since a macroscopic AFM using voice coil actuator and a permanent magnet has been developed for dynamic mode imaging previously at MIT [16], we targeted the operation in contact mode and jumping mode for this new design with a different sensing principle.

To scale up the cantilever probe, a resistive foil strain gauge is glued to the fixed end of a flexible steel ruler with 6 Hz first resonance frequency. A needle tip is glued to the free end of the cantilever ruler to interact with the sample surface. The sensing principle is similar to the piezoresistive sensor in a microscopic active probe. The resonance excitation is not needed for contact or jumping mode operation but can be added with electromagnetic actuation.

The 3-axis stepper-driven positioning system of a Creality Ender 3 3D printer is repurposed as the scanner for the macroscopic AFM. All stepper motors are rewired to external drivers and controlled using an Arduino Mega microcontroller.

For demonstration purposes, several push buttons can be used to initiate pre-programmed imaging sequences. A serial communication protocol is implemented for more advanced control of imaging parameters. The imaged data at each coordinate is both visualized on a display screen and also transmitted through serial communication.

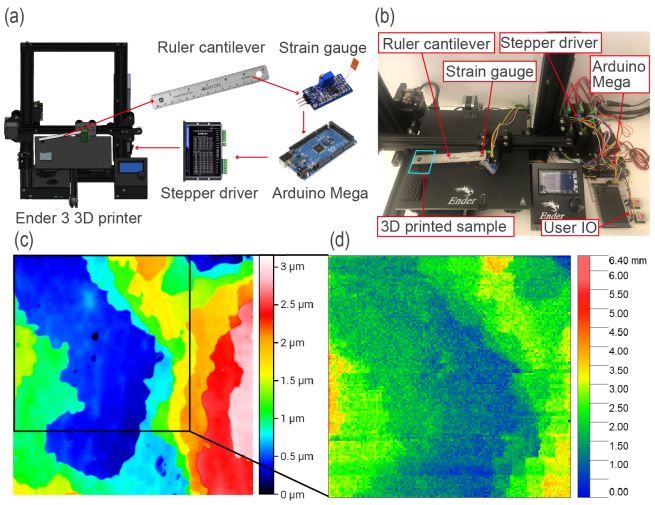


Fig. 9. Macroscopic AFM: (a) design overview main subsystems, (b) picture of the implemented system, (c) original AFM image (80 by 80 $\mu$m) and (d) topography image (25.6 by 25.6 mm) of the 3D printed seashell (400$x$ scaled) scanned using the macroscopic AFM in jumping mode

Both contact mode and jumping mode imaging controllers are implemented to regulate the deflection or maximum indentation deflection at each pixel location. For samples with high

aspect ratio, the friction force in contact mode can become a problem and the jumping mode is preferred.

The implemented system and an example scanned image of a seashell sample are shown in Fig.9(a-b). The sample is a 400$x$ scaled 3D printed surface topography of an opalescent seashell. The macroscopic AFM is set to jumping mode operation to capture the 128 by 128 pixel image with 0.2 mm in-plane scanning pixel spacing. With a single micro-step height of 0.0025 mm in the out-of-plane direction, micrometer-scale features can be resolved successfully for the sample, as shown in the comparison image in Fig.9(c-d). The macroscopic AFM as a coarse 3D profiler allows an easy understanding of the working principle of the AFM instrument and can effectively capture surface topography at the mesoscale.

### B. Haptic Force Feedback Device

The haptic force feedback device is designed to emulate both the tip-sample interaction force and cantilever resonance. Users can interact with the haptic device as if their finger is the probe. Since nanoscale interaction forces do not have good physical counterparts on the macroscopic scale, this module complements the macroscopic AFM in demonstrating force interactions in contact/dynamic modes and includes an active quality factor controller for damping adjustment. More details of the implementation can be found in [11]. Interfaces with hardware and simulated AFMs are created in this work so that forces sensed by any real AFM cantilever, the macroscopic AFM or simulated in AFM SMILER can all be emulated using the haptic device for an extended reality experience [17].

### C. Low-cost Educational AFM

A low-cost educational AFM has been developed previously to improve instrument accessibility with an easy experiment setup. The design and implemented system are shown in Fig. 10(a-b), where detailed design information can be found in reference [12]. This modular design aims to boost the availability of AFM instruments, reduce operation overhead for novice users and allow student development of the entire system for precision mechatronics education. Two upgrades are made in this work to the system including a new cantilever oscillation tapping mode demodulation scheme and a software interface to the virtual imaging module of the simulator.

For AFM tapping mode imaging, a lock-in amplifier is typically used to extract the amplitude and phase. For the active probe using piezoresistive sensor and electrothermal resonance excitation, a driving frequency $\omega$ at half of the cantilever resonance should be used, as shown in Eq.(13).

$$Z_c \propto T \propto P_{heat} = \frac{(V_{dc}+V_{ac}\sin(\omega t))^2}{R}$$
$$= \frac{1}{R}\left[V_{dc}^2 + 2V_{dc}V_{ac}\sin(\omega t) + \frac{1}{2}V_{ac}^2(1-\cos(2\omega t))\right] \quad (13)$$

where $Z_c$ is the cantilever deflection, $T$ is the probe temperature, $P_{heat}$ is the heating power, $V_{dc}$ is the offset voltage, $V_{ac}$ is the excitation voltage amplitude, $\omega$ is the excitation frequency, $t$ is time and $R$ is the heater resistance.

Since commercial lock-in amplifiers with higher harmonics demodulation capabilities are too expensive for this purpose, a custom excitation and demodulation circuit is used in the previous design. In this work, an upgrade to the system using Analog Discovery 2 (AD2) and commercially available AD630 demodulation circuit is used to replace the custom printed circuit board (PCB) for improved accessibility at an affordable cost (several hundred dollars for the modules).

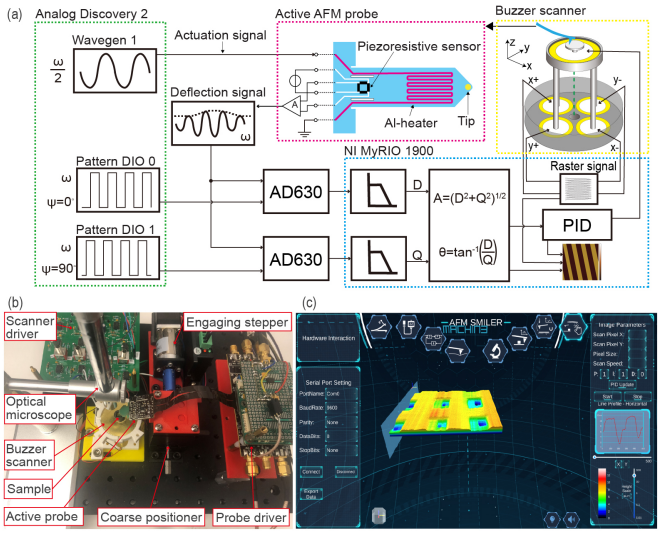


Fig. 10. Low-cost educational AFM: (a) overall system design, (b) updated signal demodulation module diagram, and (c) visualization of an imaged calibration grating in the AFM SMILER hardware interaction module

The overall signal diagram of the system is shown in Fig.10(a). Using the synchronized function generator with sine wave output at half resonance frequency $\frac{\omega}{2}$ and two channels square wave clock reference into AD630, the excitation and demodulation of the cantilever oscillation can be achieved without clock timing mismatch. Using AD2, this is achieved by configuring the WaveGen 1, Pattern DIO 0 and Pattern DIO 1 channels in the WaveForms software before the experiment. This can also be completed programmatically using LabVIEW or Matlab. Using the upgraded version, students can still obtain hands-on experience implementing the demodulation algorithm but it requires less debug effort compared to the full process of developing a custom PCB.

The AFM imaging process can also be better visualized in the AFM SMILER simulator, as shown in Fig.10(c). The scanned sample 3D view is achieved by sending the pixel height information from LabVIEW to the Unity simulator using serial communication. Users can interact with the scanned sample directly and observe the simulated image formation process in the 3D environment. The oscillation amplitude of the cantilever can also be scaled in both frequency and amplitude and reproduced on the haptic force feedback device.

## VI. Educational Studies

To verify the effectiveness of the AFM SMILER toolkit for education, two preliminary studies are conducted. First, a fifteen-minute tutorial for a basic introduction to AFM using the AFM SMILER as a virtual lab is conducted for cantilever mechanics and transducer principles. From the survey of 22 participants mostly with entry level knowledge about AFM, a score of 8.7/10 is achieved for the toolkit to help achieve better understanding of the concepts as a virtual lab. In particular, the

interaction in the simulator is more helpful than static images in the presentation slides with a preference of AFM SMILER scored at 9.0/10. The AFM SMILER software runs smoothly on participants' computer without technical issues.

Second, a nine-session workshop is offered during winter break using the developed hardware system. The workshop attracted 40 participants from a wide range of backgrounds, including mechanical engineering, electrical engineering, material science, physics, chemistry, and biology. Besides having a high score of 9.7/10 for the overall experience of the workshop for lectures, hardware lab, and AFM SMILER toolkit, all participants expressed high interest (8.8/10 score) in taking an extended version the workshop as a full semester senior/graduate level class in the future.

## VII. CONCLUSION AND FUTURE WORK

In this work, we presented the development of the AFM SMILER toolkit for interactive learning. Both scale models and extended reality hardware interaction are integrated to create the AFM digital twin. To tackle the challenges in efficient nanoscale process simulation, a combined analytical solution and numerical integration method is designed. The extended reality experience is realized by integrating the AFM SMILER software with the macroscopic AFM, the haptic force feedback device and the low-cost educational AFM. In principle, any 3D profiling system with proper communication interface can be integrated with the AFM SIMLER and the scale model digital twin scheme can be applied broadly in the field of instruments and manufacturing systems.

For future work, the AFM SIMLER will be seamlessly integrated with a book on AFM instrumentation with bidirectional interaction.Based on user feedback, a full semester class with more detailed educational studies is being designed for AFM education. Using the web version of the simulator, we will work with publishers and 3rd party platforms like nanoHub to make AFM SMILER available online for easy access to a broader audience. We are confident that the AFM SMILER toolkit can not only make an impact in precision mechatronics and instrumentation education but also benefit nanotechnology researchers who use AFM in their studies.

## ACKNOWLEDGMENT

The authors would like to acknowledge Mr. He Zeng at Lemoneko Software for Unity software support.

## REFERENCES

[1] Surya R Kalidindi et al. "digital twins for Materials". In: *Front. Mater* (2022).

[2] Faruk Ahmed Sakib, Ted Stathopoulos, and Anjan K Bhowmick. "A review of wind loads on canopies attached to walls of low-rise buildings". In: *Engineering Structures* 230 (2021), p. 111656.

[3] Zecai Lin et al. "ARei: Augmented-Reality-Assisted Touchless Teleoperated Robot for Endoluminal Intervention". In: *IEEE/ASME Transactions on Mechatronics* 27.5 (2022), pp. 3144–3154.

[4] Reza Kamali-Sarvestani et al. "Virtual Reality to Improve Nanotechnology Education: Development Methods and Example Applications". In: *IEEE Nanotechnology Magazine* 14.4 (2020), pp. 29–38.

[5] Jennifer Fromm et al. "More than experience?-On the unique opportunities of virtual reality to afford a holistic experiential learning cycle". In: *The Internet and higher education* 50 (2021), p. 100804.

[6] AH Korayem et al. "Using a virtual reality environment to simulate the pushing of cylindrical nanoparticles". In: *International journal of nanoscience and nanotechnology* 10.3 (2014), pp. 133–144.

[7] L.M. Fok, Y.H. Liu, and W.J. Li. "Modeling of Haptic Sensing of Nanolithography with an Atomic Force Microscope". In: *Proceedings of the 2005 IEEE International Conference on Robotics and Automation*. 2005, pp. 2446–2451. DOI: 10.1109/ROBOT.2005.1570479.

[8] MH Korayem et al. "Nano manipulation with rectangular cantilever of atomic force microscope (AFM) in a virtual reality environment". In: *Digest journal of nanomaterials and biostructures* 7.2 (2012), pp. 435–445.

[9] Ke Liu and Xiaobo Peng. "Simulating the approach-retract phenomenon of AFM in virtual environment with haptic interface". In: *Computer-Aided Design and Applications* 13.5 (2016), pp. 722–728.

[10] Syed Hassan et al. "Haptic guided virtual reality simulation for targeted drug delivery using nano-containers manipulation". In: *Journal of biomedical nanotechnology* 9.7 (2013), pp. 1190–1194.

[11] Fangzhou Xia et al. "Physical Intelligence in the Metaverse: Mixed Reality Scale Models for Twistronics and Atomic Force Microscopy". In: *2022 IEEE/ASME International Conference on Advanced Intelligent Mechatronics (AIM)*. 2022, pp. 1722–1729.

[12] Fangzhou Xia et al. "A modular low-cost atomic force microscope for precision mechatronics education". In: *Mechatronics* 76 (2021), p. 102550.

[13] Daniel Kiracofe et al. *VEDA: Virtual Environment for Dynamic AFM*. June 2012. DOI: doi:10.21981/THSD-5A40. URL: https://nanohub.org/resources/veda.

[14] Fangzhou Xia et al. "Model and Controller Design for High-speed Atomic Force Microscope Imaging and Autotuning". In: *Proceedings of the ASPE Spring Topical Meeting on Design and Control of Precision Mechatronic Systems*. American Society for Precision Engineering. 2020.

[15] Fangzhou Xia and Kamal Youcef-Toumi. "Advanced Atomic Force Microscopy Modes for Biomedical Research". In: *Biosensors* 12.12 (2022), p. 1116.

[16] Darya Amin-Shahidi and David Trumper. "Macro-scale atomic force microscope: An experimental platform for teaching precision mechatronics". In: *Mechatronics* 31 (2015), pp. 234–242.

[17] Guangyong Li et al. "Development of augmented reality system for AFM-based nanomanipulation". In: *IEEE/ASME Transactions on Mechatronics* 9.2 (2004), pp. 358–365. DOI: 10.1109/TMECH.2004.828651.